AIP | Journal of Applied Physics

Large magneto-electric effects in hexagonal La0.7Ba0.3MnO3-BaTiO3 solid solutions and magneto-electric coupling mechanism discussion

Qiuyun Fu, Ling Zhou, Dongxiang Zhou, Ling Miao, Chi Chen, and Fei Xue

Citation: Journal of Applied Physics **116**, 134103 (2014); doi: 10.1063/1.4897200
View online: http://dx.doi.org/10.1063/1.4897200
View Table of Contents: http://scitation.aip.org/content/aip/journal/jap/116/13?ver=pdfcov
Published by the AIP Publishing

Large magneto-electric effects in hexagonal $La_{0.7}Ba_{0.3}MnO_3$-$BaTiO_3$ solid solutions and magneto-electric coupling mechanism discussion

Qiuyun Fu,[a] Ling Zhou, Dongxiang Zhou,[a] Ling Miao, Chi Chen, and Fei Xue
School of Optical and Electronic Information, Huazhong University of Science and Technology, Wuhan 430074, People's Republic of China

(Received 1 August 2014; accepted 23 September 2014; published online 2 October 2014)

The solid solutions of $La_{0.7}Ba_{0.3}MnO_3$-$BaTiO_3$ were first prepared by a solid state method. The XRD showed that the solid solutions formed when the $BaTiO_3$ transformed from tetragonal to hexagonal phase with sintering temperature increasing. The samples with hexagonal phase exhibited relative large magneto-electric effects. For the sample sintered at 1475 °C, the measured maximum magneto-electric coefficient was 48.6 mV/cmOe, obtained at a frequency of 30 kHz. The first-principles calculations indicated that the magnetic-electric coupling was attributed to the off-centering of Mn ions in coplanar octahedrons in the hexagonal phase. The present results suggest a new candidate for a room temperature multiferroic material with magneto-electric effects.
 [http://dx.doi.org/10.1063/1.4897200]

I. INTRODUCTION

Owing to the coexistence of ferroelectricity, ferromagnetism, and magneto-electric features, there has been increasing interest in multiferroic materials, which have prospective applications in storage fields such as multi-state storage and nonvolatile magneto-electric storage units.[1,2] One category of them is ABO_3 perovskite compound materials. If the B sites are partly occupied by ferroelectric ions (Nb, W, Ta, Ti) and magnetic ions (Fe, Co, Ni, Mn) in ABO_3 compounds, the material may show ferroelectricity and magnetism simultaneously. Researchers have synthesized kinds of perovskite solid solutions with A (B, B′)O_3 (A = Ba, Pb, Bi, Sr, B = Fe, Cr, Mn, Ni, Co, B′ = Nb, W, Ta, Ti)[3–12] structure. Buscaglia[3] *et al.* have prepared $0.7BiFeO_3$–$0.3BaTiO_3$ dense ceramics with pseudocubic perovskite phase. The samples exhibit a ferro-para phase transition at around 175 °C represented by the temperature dependent dielectric constant curves. And the antiferromagnetic feature was represented by magnetic hysteresis (M-H) loops. However, their polarization-electric field (P-E) curves have not been presented. Kim[4] *et al.* have prepared ternary and binary solid solutions consisting of ferroelectric and antiferromagnetic members: $BaTiO_3$ (BTO), $PbTiO_3$, $BiFeO_3$, $PrFeO_3$, and $NdFeO_3$ samples show weak ferromagnetic feature. The maximum remanent magnetization Mr is only 0.5 emu/g appeared in the $0.8BiFeO_3$–$0.2BaTiO_3$ solid solutions, while the remanent polarization is ~1 $\mu C/cm^2$, which is obtained from the P-E hysteresis loops. Solid solution ceramics with coexistence of ferroelectricity and magnetism are also observed in $0.5(Bi_{0.9}La_{0.1})FeO_3$–$0.5Ba(Fe_{0.5}Nb_{0.5})O_3$,[5] $Pb(Zr_{0.57}Ti_{0.43})O_3$–$Pb(Fe_{2/3}W_{1/3})O_3$,[6] $0.45(Bi_{1-x}La_x)FeO_3$–$0.55PbTiO_3$,[7] $0.7Bi(Fe_{0.9}Cr_{0.1})O_3$–$0.2PbTiO_3$–$0.1BaTiO_3$,[8] $0.9BiFeO_3$–$0.1DyFeO_3$,[9] and $(1-x)Pb(Fe_{2/3}W_{1/3})O_3$-$xPb(Sc_{2/3}W_{1/3})O_3$.[10] Their multiferroic properties are represented by ferroelectric hysteresis and magnetic hysteresis, but there is no direct evidence to prove the magneto-electric coupling effects. Singh and Chatterjee[11] have prepared $LaFeO_3$-$PbTiO_3$ solid solutions with spontaneous ferroelectricity and magnetization, their magneto-electric effects represented by the magnetization comparison of the electrically poled and unpoled samples. Tripathy *et al.*[13] have observed magneto-electric coupling by frequency dependence of dielectric permittivity (ε_r) for different static magnetic field in $0.8BiFeO_3$–$0.2YMnO_3$, which has a small change of dielectric permittivity ($(\varepsilon(H)-\varepsilon(0))/\varepsilon(0)$ is ~5.5% at H = 2 T).

Generally, most of these solid solution ceramics exhibit multiferroic properties and even magneto-electric coupling effect, but due to the antiferromagnetic or weak ferromagnetic nature of $BiFeO_3$, $LaFeO_3$, $SmFeO_3$, *etc.*, the ferromagnetic and the magneto-electric effects of solid solution ceramics are not remarkable. Therefore, in this paper we tried to prepare solid solutions consisting of a strong ferromagnetic and an excellent ferroelectric material, which may induce better multiferroic and magneto-electric effects.

BTO is an outstanding ferroelectric material, which was widely used in electronic devices such as piezoelectric transducers, high permittivity capacitors, and infrared detectors due to its respective properties,[14] many researchers chose BTO to enhance the ferroelectricity and sinterability of the solid solutions ceramics. $La_{0.7}Ba_{0.3}MnO_3$ (LBMO) is a ferromagnetic material with ABO_3 (A = La, Ba; B = Mn) perovskite structure, the saturation magnetization (Ms) is ~80 emu/g (T = 5 K).[15,16] Furthermore, the LBMO compound crystallizes in a rhombohedral structure (space group R-3c) with lattice parameters a = 5.5378 Å and c = 13.5011 Å,[17] which is similar to the hexagonal $BaTiO_3$ (space group P63/mmc, a = 5.7350 Å and c = 14.0500 Å) in structure. Thus, it is possible for the two compounds to form solid solution under certain conditions. Research on this aspect has not been reported.

In this work, we have prepared LBMO-BTO solid solutions using the solid state method. The X-ray diffractograms

[a]Authors to whom correspondence should be addressed. Electronic addresses: fuqy@mail.hust.edu.cn and dxzhou@hust.edu.cn. Tel.: +86-27-87558482 and +86-18602717211. Fax: +86-27-87558482.

showed the solid solutions formed when the BTO transforms from tetragonal to hexagonal phase. The solid solution ceramics with hexagonal phase exhibit relatively large magnetic-electric (ME) effects. The ME effects are explained by the crystallographic structure of hexagonal phase and first-principles calculations in detail. The off-centering of John-Teller magnetic ions in coplanar octahedrons, which were separated by layered TiO_6 in the hexagonal phase were attributed to ME coupling effects when the external magnetic field changed.

II. EXPERIMENTAL

LBMO and BTO powders were synthesized by the solid-state reaction method and sol–gel method,[18] respectively. For LBMO, analytical-grade raw materials $KMnO_4$ and $MnCl_2{\cdot}4H_2O$ were mixed and ground in an agate mortar for 30 min, and then mixed with $BaCl_2$ and La_2O_3 (99.99%), ground with ethanol for 2 h. The mixture was dried at 70 °C, calcined at 1200 °C for 4 h in air, and slowly cooled to room temperature (RT) in the furnace. For BTO, the synthesis was followed with our previous work,[18] while the gel was dried and calcined in air at 800 °C for 2 h. The LBMO-BTO ceramics were fabricated by the conventional solid-state reaction method. LBMO and BTO powders with 0.08:0.92 mass ratios were weighed and mixed in a ball mill for 4 h, using alcohol as media. After drying, the resultant powders were pressed into pellets with a diameter of 10 mm and thickness of 1 mm at a pressure of 150 MPa, with PVA as binder. After burning off PVA at 550 °C for 30 min, the pellets were sintered at 1300–1550 °C for 2 h in air. The samples were polished and electroded with silver paste on both sides for electric tests. The crystalline phases of the powders were probed by Bruker D8 ADVANCE X-ray diffractometer (XRD) with Cu Kα radiation. The P–E hysteresis loops and leakage density measurements were obtained at RT using a Precision Ferroelectric Tester system by Radiant Technologies, Inc. The contact electrode area is 0.283 cm^2. For the ME effects measurement, two methods were applied. One was studying the effects of static magnetic field H on ferroelectric order parameters polarization, as often used in the literature.[19,20] The external dc magnetic field H was tested with a Gaussmeter (LakeShore 475 DSP Gaussmeter). The other one was the commonly α_{ME} coefficient measurement.[21,22] Before taking ME measurements, sample was poled at 120 °C at 4 kV cm^{-1} applied electric field for 1 h. The magnetic studies were carried out by Lakeshore 7400 vibrating sample magnetometer (VSM).

III. RESULTS AND DISCUSSIONS

A. Structural analysis

Figure 1 shows the XRD patterns of the sample sintered at 1300 °C, there were two perovskite phases corresponding to the tetragonal phase for BTO (Joint Committee for Powder Diffraction Standard (JCPDS) No. 01-075-0462) and rhombohedral phase for LBMO (JCPDS No. 01-089-0570), respectively. The inset of Fig. 1 is the XRD patterns of the samples sintered at of 1450, 1475, 1500, 1525, and 1550 °C.

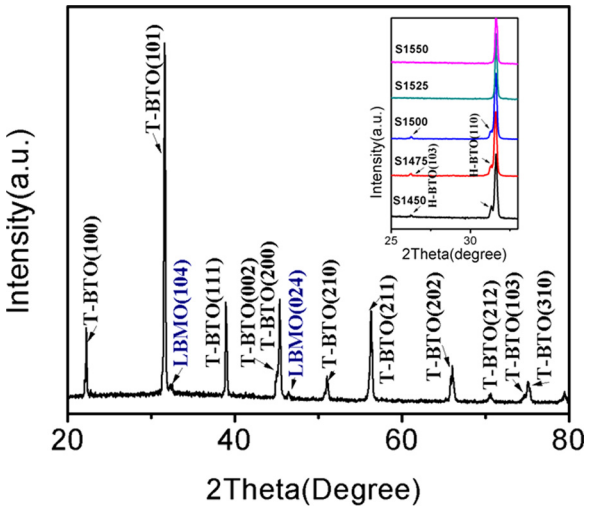

FIG. 1. X-ray diffractograms of the sample sintered at 1300 °C; the inset is the X-ray diffractograms of the samples sintered at 1450–1550 °C for 2 h.

(The samples are marked as S1450 ~ S1550.) It can be observed that as the sintering temperature rose to 1450 °C, the hexagonal BTO (H-BTO) phase generated, while the XRD peaks of rhombohedral LBMO phase disappeared, indicating that LBMO and BTO form solid solutions with hexagonal phase. With the sintering temperature increasing, the peaks of H-BTO decreased, and disappeared at 1525 °C, there remained only tetragonal phase. All the diffraction peaks of the remained tetragonal phase were between LBMO and BTO phases. It indicated that LBMO and BTO solid solutions transformed from hexagonal to tetragonal phase. Table I shows the crystal cell parameters, atom radius as well as the differences between LBMO and H-BTO. It indicates that the structure parameters of H-BTO are similar to LBMO, and meanwhile, the differences between the Ti ions and Mn^{3+}, Mn^{4+} ions are 6.6% and −12.4%, respectively. The absolute values are far below 30% beyond which the solid solutions cannot generate. Both the similarity in structure and proximity in ion radius result in the formation of substitutional solid solutions of hexagonal LBMO-BTO.

B. Ferroelectric properties and leakage current characteristic

Figure 2(a) demonstrates the P–E hysteresis loops of S1450-S1500 and S1525-S1550 (inset) at room temperature and a frequency (f) of 10 Hz. Although the applied electric field is not enough to saturate the loop, the ferroelectricity in the samples is clear. It was observed that the measured remanent polarization 2Pr of S1525 and S1550 is lower than those of S1450-S1500. Figure 2(b) shows the dc leakage current characteristic of the samples. It could be seen that all the leakage current densities were about $\sim 10^{-6}$ A/cm^2 under an electric field of 20 kV/cm. The inset of Figure 2(b) shows measured maximum leakage current density as functions of sintering temperature. With the sintering temperature increasing, the leakage current density slightly decreased, thus reduced the artificial polarization from leakage and resulted in the reduction of 2Pr of samples sintered at higher temperature.

TABLE I. Comparison of crystal cell parameters and atom radius of BTO and LBMO.

	T-BTO (01-075-0462)	H-BTO (00-008-0372)	LBMO (01-089-0570)	Differences $(P_{LBMO} - P_{H\text{-}BTO})/P_{H\text{-}BTO}$
Crystal system	Tetragonal	Hexagonal	Rhombohedral	
Space group	P4/mmm	P63/mmc	R-3c	
a	3.9945	5.7350	5.5378	−3.4%
b	3.9945	5.7350	5.5378	−3.4%
c	4.0275	14.0500	13.5011	−3.9%
α	90°	90°	90°	0
β	90°	90°	90°	0
γ	90°	120°	120°	0
B site ion radius	0.605	0.605	0.645 (Mn^{3+})	6.6%
			0.53 (Mn^{4+})	−12.4%

C. ME coupling characteristic and the ME mechanism discussion

The RT ME coupling in LBMO-BTO was also demonstrated by large electric signal measurement, studying the effects of static magnetic field H on ferroelectric order parameters polarization, as often used in the literature.[19,20] Figure 3(a) shows the P-E loops of S1475 measured under certain electric field (Electric Field = 40 kV/cm) without and with an external uniform constant applied magnetic field H (H = 200 Oe). Figure 3(b) shows changes of measured maximum polarization ΔPm ($\Delta Pm = (Pm_{200Oe} - Pm_{0Oe})/Pm_{0Oe}$) and changes of remanent polarization ΔPr ($\Delta Pr = (2Pr_{200Oe} - 2Pr_{0Oe})/2Pr_{0Oe}$) as functions of the sintering temperature. There is an obvious polarization decrease induced by the bias magnetic field in the samples S1450-S1500, which indicates certain magnetoelectric effects in the LBMO-BTO solid solution. For the sample S1475, ΔPm and ΔPr were −12.3% and −11.7%, respectively. The values are significantly higher than the values in Ref. 19 and our previous report,[20] while the applied magnetic field is lower. However, the changes drop to ∼0 for the samples S1525 and S1550. Thus, we chose S1475 to detect the ME voltage coefficient, which is defined as $\alpha_{ME} = \delta V/\delta dH_{ac}$ (d is the thickness of disk). The ME measurements were carried out by applying both H_{dc} and small H_{ac} parallel to the disk plane. Figure 3(c) shows the frequency dependence of measured α_{ME} values by applying an AC magnetic field ΔH_{ac} (3.5 Oe) at RT. The AC magnetic field frequency was varied from 1 KHz to 100 kHz. It can be observed that the α_{ME} coefficient of S1475 increases with the increasing of the frequency and reach the maximum value at 30 kHz, and then decreases. The results suggest that resonant frequencies are near 30 kHz. The inset of Figure 3(c) shows the ME voltage coefficient α_{ME} as a function of DC bias magnetic field H_{dc} at $H_{ac} = 3.5$ Oe and f = 30 kHz. The result indicates that the ME sensitivity of S1475 is strongly dependent on H_{dc}. At a bias field of $H_{dc} = 0$, the sample has a remanent induction. The initial application of the DC field removes this remanent induction, and thus makes α_{ME} decrease to a minimum until induction is reduced to zero at the coercive field.[21] As H_{dc} increases, α_{ME} increases but owing to the limitation of DC field, the value does not reach the peak. The measured maximum α_{ME} value is 48.6 mV/cmOe with $H_{dc} = 0$, and it is suggested to be larger if higher DC field is applied. The value is higher than bulk $BiFeO_3$ (Ref. 23) and even some composite multiferroics[21] at RT. For comparison, we have measured the α_{ME} of S1550 (not shown here), the value hardly vary with DC field, which corresponding to the non-variation of P-E loops without and with a magnetic field. In order to detect the multiferroic feature of S1475, we have measured the M-H loops at RT, as shown in Figure 3(d). The saturation magnetization (Ms), remanent magnetization (Mr), and coercivity (Hc) are 1.21 emu/g, 3.26 memu/g, and 10.85 Oe, respectively. Even though the sample show a weak ferromagnetic behavior, combined with the ferroelectric feature, S1475 exhibits a typical multiferroic feature with strong ME coupling effects.

The ME coupling measurement inferred that the samples sintered at 1450 °C to 1500 °C where the solid solutions structured in hexagonal phase exhibit ME effects, while the samples sintered at 1525 °C to 1550 °C where the solid

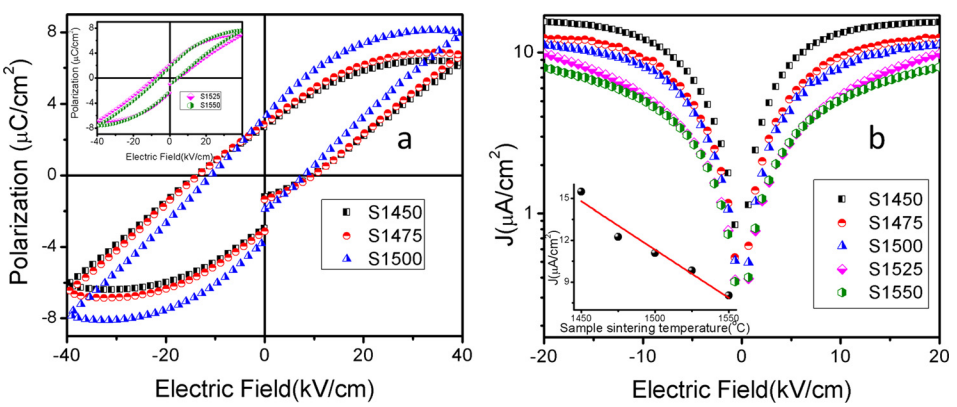

FIG. 2. (a) P–E hysteresis loops of S1450-S1500 solid solutions ceramics measured at RT, the inset is the P–E hysteresis loops of S1525-S1550 and (b) leakage current characteristic of LBMO-BTO solid solutions; the inset is the leakage current density measured at 20 kV/cm as functions of sintering temperature.

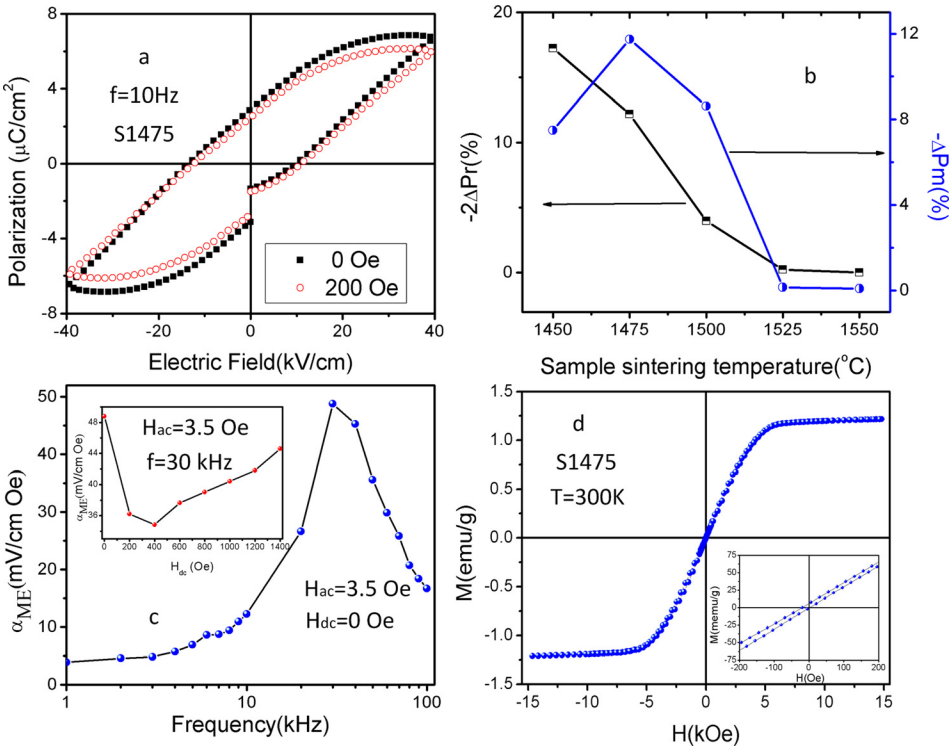

FIG. 3. (a) RT P–E hysteresis loops without and with an external magnetic field for sample S1475, (b) ΔPm and ΔPr as functions of the sintering temperature, (c) the frequency dependence of measured α_{ME} values for S1475; the inset is the ME voltage coefficient α_{ME} as a function of DC bias magnetic field H_{dc} at $H_{ac} = 3.5$ Oe and $f = 30$ kHz. (d) the magnetic hysteresis loops of S1475 measured at RT.

solutions structured in tetragonal phase hardly show ME effects. Figure 4(a) shows the crystallographic structure of hexagonal BTO. It can be seen from the figure that Ti atoms situate at the centers of independent oxygen octahedrons (Ti1, in blue polyhedron) and coplanar octahedrons (Ti2, in orange polyhedron). The lengths of Ti-O bonds are given in Table II. It can be seen from the table that independent oxygen octahedrons is central-symmetrical, while the coplanar octahedrons is non-central-symmetrical. In order to confirm which situation of Ti is easier to be substituted, we have accomplished first-principles calculations.

The first-principles calculations are performed using VASP code[24] and based on density-functional theory (DFT).[25,26] The exchange–correlation energy is calculated using general gradient approximation (GGA).[27] The electron wave function was expanded in plane waves up to a cutoff energy of 400 eV and a k-point mesh of $4 \times 4 \times 2$ in the Monkhorst Pack[28] sampling scheme are used for geometry optimization and $8 \times 8 \times 4$ for electronic property calculations. The structural relaxation is performed until the forces on all the atoms are less than 0.02 eV/Å. And spin polarization is considered in the calculations. By calculations, the total energy of Mn substituted Ti1 is −235.326675 eV, while that of Mn substituted Ti2 is −235.768648 eV. Thus, it could be concluded that Ti2 site is more suitable for Mn to substitute in $BaTiO_3$ for the lower total energy.

To understand the bonding and origin of the electric polarization, the total charge density for a-b plane of Mn substituted Ti1 (upper) and Ti2 (lower) in H-BTO was shown in Figure 4(b). From the figure, we can see the significant asymmetry of the Mn-O bond length in the Mn substituted Ti2 H-BTO. This shows the origin of the electric polarization. The Mn-O bond length of Mn substituted $BaTiO_3$ is shown in Table II. The average Mn-O bond length is shorter than Ti-O bond length, which indicates higher chemical interaction. And it is worth mentioning that Mn substituted BTO aggravated the non-central-symmetry of the coplanar octahedrons. The ΔL ($(L_{min} - L_{max})/L_{max}$) of Ti-O

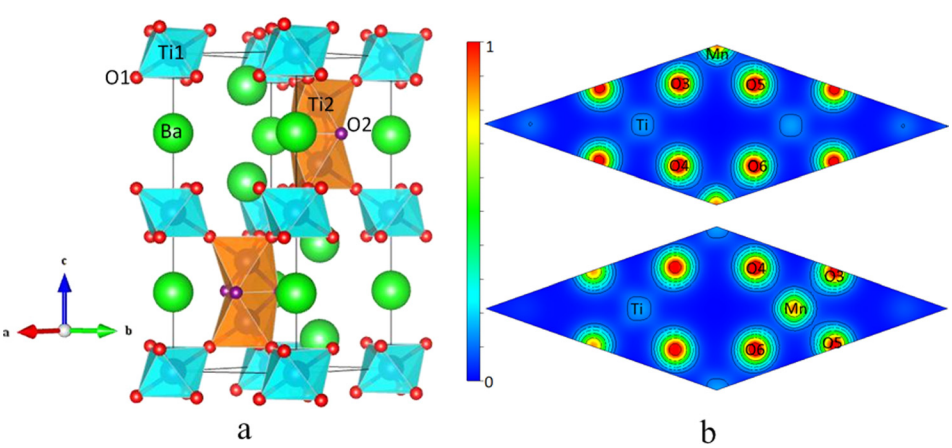

FIG. 4. (a) Crystal structure of hexagonal $BaTiO_3$ (the green, purple, and red spheres denote Ba, O1, and O2 atoms, respectively. Spheres situated in blue and orange polyhedron are Ti1 and Ti2 atoms.), and (b) 2D charge density plots in atomic units obtained from a DFT calculation for the a–b plane of the Mn substituted Ti1 (upper) and Ti2 (lower) in H-BTO.

TABLE II. Ti/Mn-O bond lengths in $BaTiO_3$ and $Ba(Ti,Mn)O_3$.

	Ti-O1	Ti-O2	Ti-O3	Ti-O4	Ti-O5	Ti-O6	$\Delta L\ (L_{min}-L_{max})/L_{max}$
$BaTiO_3$-Ti1	1.94783	1.94783	1.94783	1.94783	1.94783	1.94783	0
$BaTiO_3$-Ti2	2.01525	1.96127	1.96127	2.01525	1.96127	2.01525	−2.7%
	Mn-O1	Mn-O2	Mn-O3	Mn-O4	Mn-O5	Mn-O6	
Mn substitute Ti2	1.88974	1.93633	1.90306	1.97193	1.90306	1.97193	−4.2%

bond length in BTO is −2.7%, while the ΔL of Mn-O bond length in Mn substituted BTO is −4.2%.

Thus, when a portion of tetragonal BTO transformed to hexagonal BTO with the sintering temperature rise, LBMO-BTO substitution solid solution is formed. A sites are occupied by Ba and La, B sites are occupied by Ti and Mn. 70% of Mn ions possess 3+ oxidation state and 30% Mn ions possess 4+ oxidation state. Mn substituted Ti2 randomly, formed non-central-symmetry $Mn_xTi_{(2-x)}O_9$ (x = 1,2) coplanar octahedrons along c axis. The $Mn_xTi_{(2-x)}O_9$ coplanar octahedrons were separated by layered independent oxygen octahedrons TiO_6. The non-central-symmetry of the coplanar octahedrons with a polar direction parallel to c axis is the key structural reason for materials exhibiting ferroelectricity.[29] However, it was structurally different from that of other hexagonal perovskites in which ferroelectricity was driven by the bulking of the layered MnO_5 polyhedron in $YMnO_3$ (Refs. 30 and 31) and $TmMnO_3$.[32] When an external magnetic field was applied, the spin state of Mn^{3+} was changed and John-Teller effect of Mn^{3+} was promoted, which induced the lattice distortion and led to the ME coupling effects as shown in Fig. 4. As the temperature rises, the hexagonal phase transformed to tetragonal phase, Mn-O bonds tended to be more symmetrical, and the changes tended to be weaker.

The key points of the origin of multiferroic and ME effects are the non-central-symmetric coplanar octahedrons in hexagonal structure and the existence of John-Teller ions Mn^{3+}. The multiferroic of non-central-symmetric coplanar octahedrons in hexagonal structure has been reported in 2H-$BaMnO_3$ in Refs. 33 and 34. The authors theoretically suggested that the antiferromagnetic 2H-$BaMnO_3$ would be a potential material exhibiting ferroelectric features owing to its face-sharing octahedral in the hexagonal structure. Satapathy[35] has reported that the 2H-$BaMnO_3$ represented weak relaxor characteristic through dielectric diffusivity calculated from modified Curie-Weiss laws and nonlinear Vogel-Fulcher fittings. And the author considered that the presence of a smaller amount of Mn^{3+} cations created disorder in 2H-BaMnO3 and led to the weak relaxor properties. However, there is no direct evidence to prove the ferroelectricity and ME coupling effects in hexagonal structure with coplanar octahedrons. Our work has just experimentally proved that when the John-Teller magnetic ions occupy the center of coplanar octahedrons in hexagonal structure, they might induce ME coupling effects. In fact, we have prepared several groups of x LBMO-(1 − x) BTO (x = 0.16, 0.24, 0.32) solid solutions. But the samples prepared with more LBMO exhibited large leakage current density ($\sim10^{-4}$, $\sim10^{-3}$, and $\sim10^{-1}$ A/cm^2 for x = 0.16, x = 0.24 and 0.32, respectively) and thus hardly obtained effective P-E hysteresis loops. We suggest that with the increasing of LBMO, not only Ti2 but also Ti1 will be substituted in the hexagonal phase and form a Mn-O-Mn-O-Mn chain, which is unlike the Ti-O-Mn-O-Mn(Ti)-Ti chain in solid solutions with lower LBMO. Owing to the double exchange between Mn^{3+} and Mn^{4+}, the solid solutions will be transformed to ferromagnetic metallic state, which leads to a high leakage current density consequently. This may be the reason of why there is no P-E hysteresis loops observed in pure 2H-$BaMnO_3$ for its Mn-O-Mn chain along c axis.

IV. CONCLUSIONS

In conclusion, we have first prepared the LBMO-BTO solid solutions. The solid solutions formed when the BTO transforms from tetragonal to hexagonal phase. The solid solutions with hexagonal phase exhibit relatively large ME effects. The α_{ME} coefficient is 48.6 mV/cmOe. The ME effects are explained by the crystallographic structure of hexagonal phase and first-principles calculations in detail. Our work suggests that the hexagonal single phase materials with John-Teller magnetic ions in coplanar octahedrons but without magnetic ions chain will be potential multiferroics. We hope that our work will motivate the search of new multiferroics in this class of compounds.

ACKNOWLEDGMENTS

The authors are grateful for financial supports from the National Nature Science Foundations of China under Grant No. 60871017 and the National High Technology Research and Development Program of China (863 Program) under Grant No. 2013AA030903.

[1]J. F. Scott, Nature Mater. **6**, 256–257 (2007).
[2]M. Bibes and A. Barthelemy, Nature Mater. **7**, 425–426 (2008).
[3]M. T. Buscaglia, L. Mitoseriu, V. Buscaglia, I. Pallecchi, M. Viviani, P. Nanni, and A. S. Siri, J. Eur. Ceram. Soc. **26**, 3027–3030 (2006).
[4]J. S. Kima, C. I. Cheona, P. W. Jang, Y. N. Choi, and C. H. Lee, J. Eur. Ceram. Soc. **24**, 1551–1555 (2004).
[5]H. Paik, H. Hwang, K. No, S. Kwon, and D. P. Cann, Appl. Phys. Lett. **90**, 042908 (2007).
[6]D. Lee, Y.-A. Park, S. M. Yang, T. K. Song, Y. Jo, N. Hur, J. H. Jung, and T. W. Noh, J. Phys. D: Appl. Phys. **43**, 455403 (2010).
[7]J. R. Cheng, S. W. Yu, J. G. Chen, Z. Y. Meng, and L. E. Cross, Appl. Phys. Lett. **89**, 122911 (2006).
[8]X. H. Liu, Z. Xu, X. Y. Wei, and X. Yao, J. Am. Ceram. Soc. **93**, 1245–1247 (2010).
[9]W. M. Zhu, L. W. Su, Z. G. Ye, and W. Ren, Appl. Phys. Lett. **94**, 142908 (2009).
[10]R. Wongmaneerung, X. Tan, R. W. McCallum, S. Ananta, and R. Yimnirun, Appl. Phys. Lett. **90**, 242905 (2007).
[11]A. Singh and R. Chatterjee, Appl. Phys. Lett. **93**, 182908 (2008).

[12]X. Peng, H. J. Kang, L. J. Liu, C. Z. Hu, L. Fang, J. Chen, and X. R. Xing, Solid-State Sci. **15**, 91–94 (2013).
[13]S. N. Tripathy, K. K. Mishra, S. Sen, B. G. Mishra, D. K. Pradhan, R. Palai, and D. K. Pradhan, J. Appl. Phys. **114**, 144104 (2013).
[14]G. H. Haertling, J. Am. Ceram. Soc. **82**(4), 797–818 (1999).
[15]H. L. Ju, Y. S. Nam, J. E. Lee, and H. S. Shin, J. Magn. Magn. Mater. **219**, 1–8 (2000).
[16]H. S. Im, G. B. Chon, S. M. Lee, B. H. Koo, C. G. Lee, and M. H. Jung, J. Magn. Magn. Mater. **310**, 2668–2670 (2007).
[17]P. G. Radaelli, M. Marezio, H. Y. Hwang, and S.-W. Cheong, J. Solid State Chem. **122**, 444–447 (1996).
[18]D. X. Zhou, G. Jian, Y. X. Hu, Y. N. Zheng, S. P. Gong, and H. Liu, Mater. Chem. Phys. **127**, 316–321 (2011).
[19]G. Sreenivasulu, M. Popov, F. A. Chavez, S. L. Hamilton, P. R. Lehto, and G. Srinivasan, Appl. Phys. Lett. **104**, 052901 (2014).
[20]G. Jian, D. X. Zhou, J. Y. Yang, H. Shao, F. Xue, and Q. Y. Fu, J. Eur. Ceram. Soc. **33**, 1155–1163 (2013).
[21]Z. H. Tang, Y. Xiong, M. H. Tang, Y. G. Xiao, W. Zhang, M. L. Yuan, J. Ouyang, and Y. C. Zhou, J. Mater. Chem. C **2**, 1427 (2014).
[22]B. Tong, X. F. Yang, Z. Guo, K. Li, J. Ouyang, G. Q. Lin, and S. Chen, Ceram. Int. **39**, 6853–6859 (2013).
[23]J. M. Caicedo, J. A. Zapata, M. E. Gómez, and P. Prieto, J. Appl. Phys. **103**, 07E306 (2008).
[24]G. Kresse and J. Hafner, Phys. Rev. B **49**, 14251–14269 (1994).
[25]P. Hohenberg and W. Kohn, Phys. Rev. **136**, B864–B871 (1964).
[26]W. Kohn and L. J. Sham, "Self-consistent equations including exchange and correlation effects," Phys. Rev. **140**, A1133–A1138 (1965).
[27]J. P. Perdew, K. Burke, and M. Ernzerhof, Phys. Rev. Lett. **77**, 3865 (1996).
[28]H. J. Monkhorst and J. D. Pack, Phys. Rev. B **13**, 5188–5192 (1976).
[29]W. Prellier, M. P. Singh, and P. Murugavel, J. Phys.: Condens. Matter **17**, R803–R832 (2005).
[30]D. G. Tomuta, S. Ramakrishnan, G. J. Nieuwenhuys, and J. A. Mydosh, J. Phys.: Condens. Matter **13**, 4543–4552 (2001).
[31]B. B. Vanaken, T. T. M. Palstra, A. Filippetti, and N. Spaldin, Nature Mater. **3**, 164–170 (2004).
[32]L. J. Wang, S. M. Feng, J. L. Zhu, R. C. Yu, C. Q. Jin, W. Yu, X. H. Wang, and L. T. Li, Appl. Phys. Lett. **91**, 172502 (2007).
[33]J. M. Rondinelli, A. S. Eidelson, and N. A. Spaldin, Phys. Rev. B **79**, 205119 (2009).
[34]J. Varignon and P. Ghosez, Phys. Rev. B. **87**, 140403(R) (2013).
[35]S. Satapathy, M. K. Singh, P. Pandit, and P. K. Gupta, Appl. Phys. Lett. **100**, 042904 (2012).